THE JOURNAL OF PHYSICAL CHEMISTRY Letters

Letter

Cite This: J. Phys. Chem. Lett. 2019, 10, 6246−6252

pubs.acs.org/JPCL

Complex Optical Conductivity of Two-Dimensional MoS_2: A Striking Layer Dependency

Baokun Song,[†] Honggang Gu,*[,†] Mingsheng Fang,[†] Yen-Teng Ho,[‡] Xiuguo Chen,[†] Hao Jiang,[†] and Shiyuan Liu*[,†]

[†]State Key Laboratory of Digital Manufacturing Equipment and Technology, Huazhong University of Science and Technology, Wuhan 430074, Hubei, China

[‡]Department of Materials Science and Engineering, National Chiao Tung University, Hsinchu 30010, Taiwan, China

Supporting Information

ABSTRACT: The complex optical conductivities of two-dimensaionl (2D) materials are fundamental for extended applications of related optoelectronic devices. Here, we systematically investigate the layer-dependent evolutions in the complex optical conductivities of 1−6 layer 2D MoS_2 over an ultrawide spectral range (0.73−6.42 eV) by spectroscopic ellipsometry. We identify five feature peaks (A−E) in the optical conductivity spectra, which present interesting layer dependencies due to the scaling effect. Results suggest that the center energies of peaks A and B are nearly layer-independent, while those of peaks C and D exhibit redshifts as the layer increases. We interpret these layer-dependent evolutions as the competition between the decreasing exciton effect and the prominent band shrinkage with the increasing layer number. Additionally, the applicability of the classical slab model and the surface current model in evaluating the optical conductivities of 2D MoS_2 with different layers is discussed from an experimental perspective.

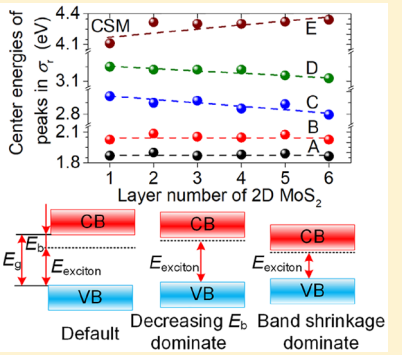

Two-dimensional (2D) materials, such as graphene, transition metal dichalcogenides (TMDCs), hexagonal boron nitride, etc., have received intense interest in many fields, covering condensed matter physics, material sciences, and optoelectronics.[1−3] In comparison with the zero-gap graphene, 2D TMDCs are more suitable for applications in the new type of optoelectronic and nanoelectronic devices because of their widely tunable band gaps and relatively high carrier mobility.[4−6] Among various 2D TMDCs, the 2D MoS_2 is the first one fabricated in laboratories and has been widely introduced into many devices.[7−9] The performances of these MoS_2-based devices are closely related to the inherent optical properties of 2D MoS_2.[10,11] The complicating factor is that the optical properties of 2D MoS_2 are sensitive to the layer number, which makes it more challenging to predict the performances of those devices.[12] For instance, the size and type of the band gap have been confirmed to be dependent on the layer number of MoS_2.[13] To provide a parametrized guidance for the design and optimization of MoS_2-based devices, it is crucial to accurately and comprehensively characterize the optical properties of 2D MoS_2.

Generally, there are three pairs of complex parameters that can be used unambiguously to evaluate the optical properties of an optoelectronic material, namely, the dielectric function $\varepsilon = \varepsilon_r - i\varepsilon_i$, the complex refractive index $N = n - i\kappa$ (n and κ refer to the refractive index and the extinction coefficient, respectively), and the complex optical conductivity $\sigma = \sigma_r + i\sigma_i$. The dielectric function and the complex refractive index of 2D MoS_2 have been widely studied by various techniques, such as ellipsometry, reflection/absorption spectrometry, and the optical contrast method.[12,14−20] In contrast, the complex optical conductivity is directly related to the photocurrent and photoresistance, which is highly desirable for the development of relevant optoelectronic devices, especially photoconductors, photovoltaics, photodetectors, etc.[21−23] However, there is little reported research that provides a systematic investigation into the complex optical conductivity of 2D MoS_2 with different layers because of the controversy involving optical modeling and the lack of sufficient high-quality and layer-controlled 2D MoS_2 samples.[24,25] At present, two main models are used to obtain the optical conductivity of 2D materials. The first one is the classical slab model (CSM), in which the 2D material is regarded as a homogeneous slab with a finite thickness.[26] The second one is called the surface current model (SCM), in which the 2D material is treated as an infinitely thin sheet with light-induced surface currents.[27,28] In the CSM, both the interface effect and propagation effect of the polarized light reacting with the 2D materials are taken into account, where the thickness of the 2D material is involved. In the SCM, only the reaction between the polarized light and the 2D material at the interface is considered.

Following the basic principle of the CSM, the reflectance spectrum of the mechanical exfoliated monolayer MoS_2 under normal incidence was measured by Li et al., and the real part of

Received: July 19, 2019
Accepted: August 27, 2019
Published: September 6, 2019

DOI: 10.1021/acs.jpclett.9b02111
J. Phys. Chem. Lett. 2019, 10, 6246−6252

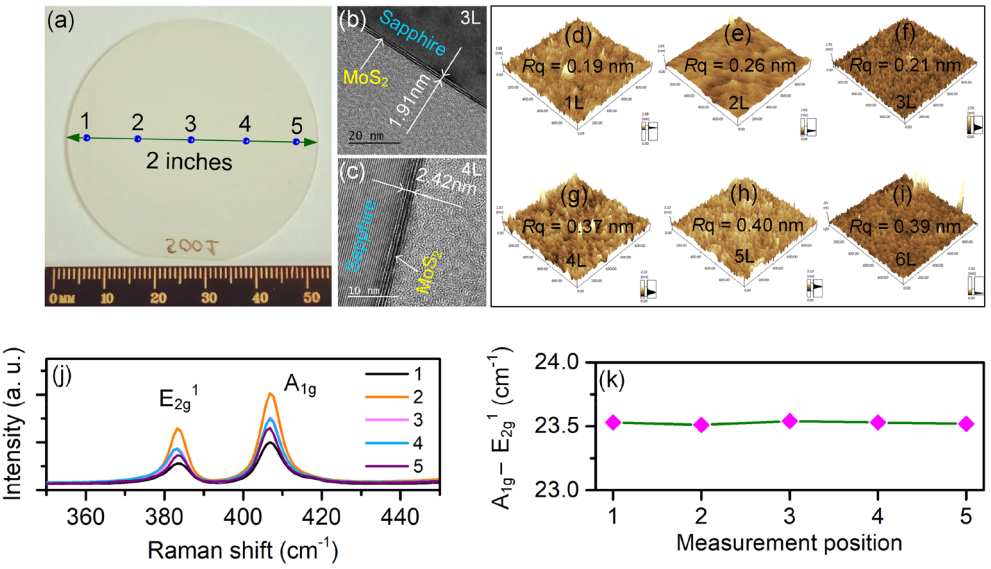

Figure 1. (a) Photograph of the 2 in. 3L MoS_2 on sapphire substrate prepared by the two-step method. (b and c) Cross-sectionsl TEM images of 3L and 4L MoS_2. The thicknesses of these two samples are 1.91 and 2.42 nm, respectively. (d–i) AFM images and surface roughness of 1–6L MoS_2. The scanning area is 1 μm × 1 μm. (j) Raman spectra of five testing points along the diameter of the 3L MoS_2 wafer. The wavelength of the detection laser is 532 nm. (k) Frequency differences between the A_{1g} and E_{2g}^1 Raman peaks.

the in-plane complex optical conductivity of the monolayer MoS_2 was calculated.[18] This measurement approach can be traced to the work conducted by Liang,[29] in which the bulk transition metal dichalcogenides were regarded as uniaxial anisotropic materials and the in-plane and out-of-plane reflectivity was measured. Jia et al. extracted the complex optical conductivities of 2D MoS_2 with different layers over the energy range of 1.5–3.0 eV from the reflectance R and the transmittance T at normal incidence,[26] and these R and T were calculated by using reported complex refractive indices of 2D MoS_2.[15] Morozov et al. obtained the complex optical conductivity of the monolayer MoS_2 from measured R and T by using the SCM without involving the thickness.[30] Using a nondegenerate ultrafast optical pump–probe technique, Wang et al. obtained the transient complex optical conductivity of 3–27 layer MoS_2 films.[31] In addition, some researchers were devoted to predicting the complex optical conductivity of 2D MoS_2 by using first-principles calculations.[32,33] In summary, most of the studies mainly focus on the optical conductivity of the monolayer 2D MoS_2 over a narrow spectral range. The layer-dependent complex optical conductivity of 2D MoS_2 over a wide spectral range has not yet been investigated adequately, particularly from the view of experiments. Moreover, the existing results remain inconsistent and controversial,[24,26–28] and the applicability of the CSM and the SCM in evaluating the complex optical conductivities of a 2D material needs to be experimentally discussed.

In this work, we systematically investigate the layer-dependent evolutions in the complex optical conductivities of 2D MoS_2 films over an ultrabroad energy range (0.73–6.42 eV) by spectroscopic ellipsometry (SE). Wafer-scale, high-quality, layer-controllable 2D MoS_2 thin films with different layers are prepared on the sapphire substrates by the two-step method. The complex optical conductivities are comparatively evaluated by the SCM and the CSM from the measured ellipsometric parameters and the extracted complex refractive index, respectively. The applicability of the SCM and the CSM in evaluating the optical conductivity of 2D MoS_2 is discussed according to the experimental results. Up to five intrinsic feature peaks (A–E) are found in the complex optical conductivity spectra of 2D MoS_2 over the concerned spectral range, which can be attributed to the interband optical transitions and exciton transitions. More importantly, we study the layer dependencies found in the optical conductivity over the ultrabroad energy range (0.73–6.42 eV) and reveal the underlying physical mechanisms forming these evolutions.

Wafer-scale, high-quality, layer-controllable 2D MoS_2 is prepared by an approach called the two-step method.[12,34] Detailed fabrication processes can be found in Experimental Methods. Figure 1a illustrates a photograph of a 3L 2D MoS_2 on the 2 in. sapphire wafer. The uniform optical contrast indicates that the MoS_2 film prepared by us exhibits an extremely uniform thickness over the entire wafer scale. As shown in Figure 1b,c, the thicknesses of the 2D MoS_2 are determined by high-resolution transmission electron microscopy (TEM). The clear layered structures shown in the TEM images indicate that the 2D MoS_2 are of high crystal quality. The surface roughness of these 2D MoS_2 samples is measured by the atomic force microscope as shown in Figure 1d–g, and the R_q for all of these specimens is lower than 0.4 nm, indicating the samples have excellent flatness. The Raman spectra of five points along the diameter of the 3L MoS_2 wafer as shown in Figure 1a are measured and plotted in Figure 1h. The frequent differences between the two typical Raman peaks A_{1g} and E_{2g}^1 are stable at 23.5 cm^{-1} (Figure 1i), which is consistent with the result of the mechanical exfoliated 3L MoS_2.[35,36] In addition, the full width at half maximums of the Raman peaks of the 2D MoS_2 prepared by us are as narrow as those of the mechanical exfoliated 2D MoS_2.[36] The measurement results from the Raman spectroscopy confirms that the 2D MoS_2 prepared by us presents excellent crystal quality and uniformity.

The ellipsometric spectra of the 2D MoS_2 are measured by a commercial ellipsometer, and the complex refractive indices of the 2D MoS_2 are obtained by performing the ellipsometric analysis. The basic principles of ellipsometry and the

DOI: 10.1021/acs.jpclett.9b02111
J. Phys. Chem. Lett. 2019, 10, 6246–6252

experimental setup together with the detailed ellipsometric analysis procedures can be found in the Supporting Information (Figures S1 and S2) and previous publications.[37−40] The measured ellipsometric spectra and the extracted complex refractive indices of 2D MoS_2 with different layers are presented in Figures S3 and S4. In this work, the CSM and SCM are adopted to comparatively evaluate the complex optical conductivity of 2D MoS_2. In the CSM, the 2D material is considered as a slab with finite thickness d as shown in Figure 2a, and the complex optical conductivity can be calculated by the complex refractive index and thickness[18,28,33]

$$\sigma_{2D}(\omega) = id\varepsilon_0\omega[N_{2D}{}^2(\omega) - 1] \quad (1)$$

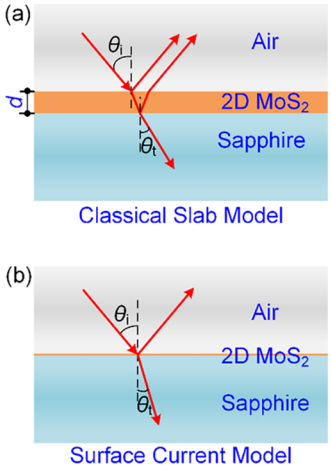

Figure 2. Schematic diagrams for the optical models of 2D MoS_2 on the sapphire substrate: (a) the classical slab model and (b) the surface current model.

where d and N_{2D} are the thickness and the complex refractive index of the 2D material, respectively; ε_0 and ω stand for the free-space permittivity and the angular frequency of the light, respectively. In contrast, in the SCM, a truly 2D material is regarded as an infinite thin interface as shown in Figure 2b,[27] and the complex optical conductivity can be extracted directly from the measured ellipsometric parameters without involving the thickness[24,27]

$$\tan\Psi\cdot\exp(i\Delta) = \frac{N_2C_i - N_1C_t + (i\sigma_i/\varepsilon_0\omega + \sigma_rZ_0)C_iC_t}{N_2C_i + N_1C_t + (i\sigma_i/\varepsilon_0\omega + \sigma_rZ_0)C_iC_t} \cdot \frac{N_1C_i + N_2C_t + i\sigma_i/\varepsilon_0\omega + \sigma_rZ_0}{N_1C_i - N_2C_t - i\sigma_i/\varepsilon_0\omega - \sigma_rZ_0} \quad (2)$$

where Ψ and Δ are ellipsometric parameters and $Z_0 = 120\pi\ \Omega$ represents the vacuum impedance; N_1 and N_2 are the complex refractive indices of the superstrate and the substrate of the 2D material, respectively. In the case of Figure 2b, $N_1 = N_{Air} = 1$ and $N_2 = N_{Sapphire}$. $N_{Sapphire}$ can be determined by the SE $C_i = \cos\theta_i$ and $C_t = \cos\theta_t$, where θ_i and θ_t represent the incident angle and refractive angle in the substrate, respectively.

Figure 3a,b comparatively presents complex optical conductivities of the 2D MoS_2 with different layers evaluated by the CSM and the SCM, which have been normalized by $2e^2/h$ (e and h refer to the electron charge and the Planck constant). The sign of σ_i under 2.74 eV in our work is contrary to the result given by Wang et al.[31] The negative σ_i observed by Wang et al. could partly be attributed to the significantly decreased mobility of charge carriers, because recombination of photoexcited carriers under ultrafast optical pump−probe beams can increase the carrier effective mass and the scattering probability.[26] Five obvious feature peaks (labeled with uppercase letters A−E) can be observed in the optical conductivity spectra. The inset in Figure 3a illustrates the band structure of the 2D MoS_2, and the optical transitions occurring at these feature peaks are specified. The direct

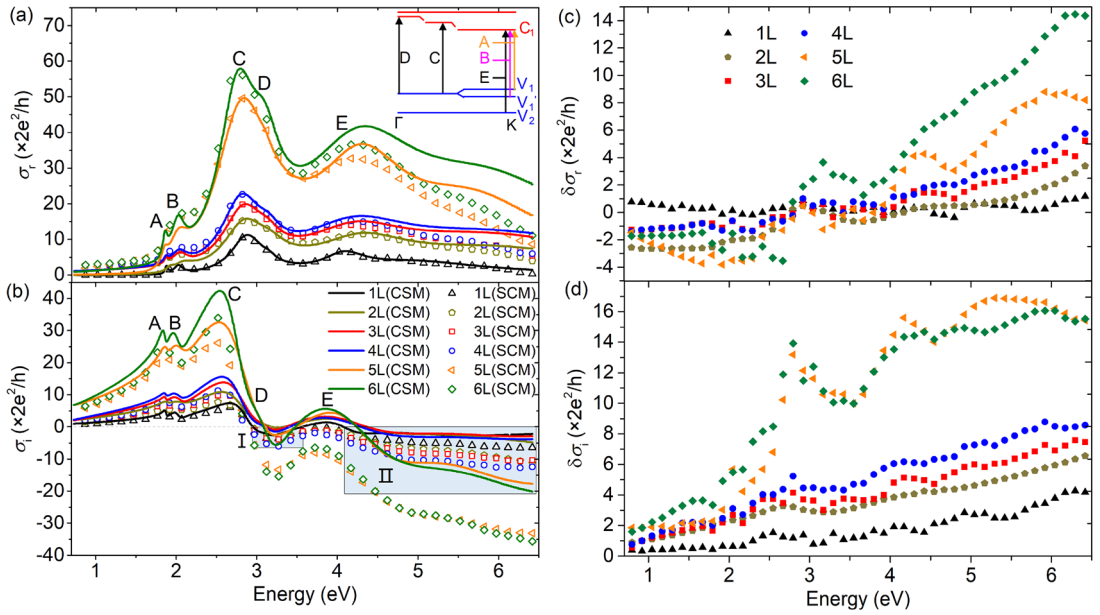

Figure 3. Complex optical conductivities of 1−6L MoS_2: (a) real part (σ_r) and (b) imaginary part (σ_i). The inset in panel a is the schematic (not to scale) of the band structure of 2D MoS_2. (c and d) Differences of the complex optical conductivities calculated by CSM and SCM. The vertical coordinate $\delta\sigma_r = \sigma_r^{CSM} - \sigma_r^{SCM}$ ($\delta\sigma_i = \sigma_i^{CSM} - \sigma_i^{SCM}$), where σ_r^{CSM} (σ_i^{CSM}) and σ_r^{SCM} (σ_i^{SCM}) stand for the real (imaginary) parts of the complex optical conductivities obtained from the CSM and the SCM, respectively.

DOI: 10.1021/acs.jpclett.9b02111
J. Phys. Chem. Lett. 2019, 10, 6246−6252

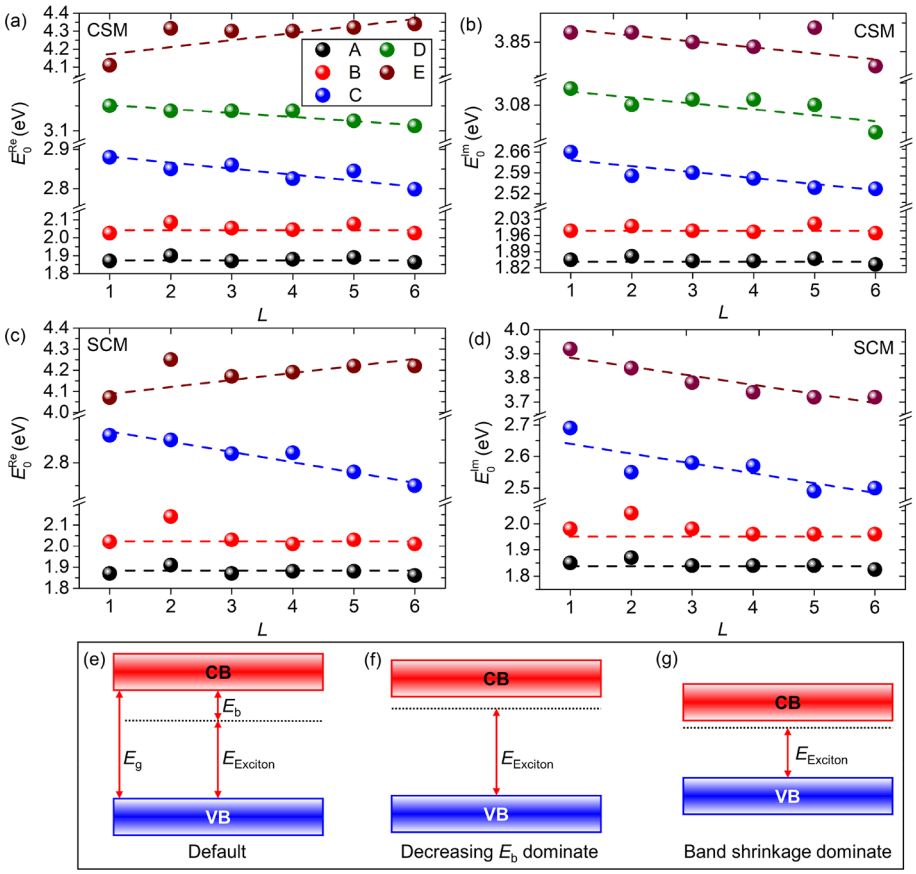

Figure 4. (a and b) Center energies of feature peaks A−E in the CSM-calculated complex optical conductivity versus the layer number of 2D MoS_2. (c and d) Center energies of feature peaks A, B, C, and E in the SCM-calculated complex optical conductivity versus the layer number of 2D MoS_2. Dashed lines in the panels a−d are just drawn as a guide to the eye. (e−g) Schematic diagrams of the competition mechanisms between the decreasing exciton binding energy and the band shrinkage. (e) Default local electronic band structure of the monolayer 2D MoS_2 with exciton ground state (blue line between the CB and the VB). (f) The decreasing E_b dominates $E_{Exciton}$. (g) The band shrinkage dominates $E_{Exciton}$.

transitions between the split valence bands (VB_1 and VB_1') and the first conduction band (CB_1) lead to the formations of the CPs A and B, which occur at the K point of the brillouin zone (BZ). The physical origins of peaks C and D are similar, which mainly stem from the particle−hole excitations between approximately parallel bands (VB_1 and CB_1) apart along the Γ−K symmetry line in the BZ.[12,32] In other words, in this region of the BZ, the prominent band nesting induces singularities of the joint density of state and further leads to the high optical conductivity.[41] The high-energy peak E can be understood as the optical transitions from VB_2 to CB_1.[12] In addition, it can be observed that there are two regions [(I) 2.95−3.58 eV and (II) 4.10−6.42 eV, highlighted by the blue background] where the imaginary parts of the complex optical conductivities σ_i are negative. This is expected to render some novel insights for the design of MoS_2-based metamaterials and sensors.[27,42,43] Specifically, the negative σ_i is mainly from the partial plasma resonance. It can be attributed to the saturation of the four unoccupied "d" bands (there are 18 valence electrons), which are separated by a small gap or a density-of-states minimum from the "s/p" conduction bands at higher energies (see Figure 5 in ref 44).[44,45] The plasma response generally exhibits a polarization-dependent absorption feature. Thus, the polarization-dependent absorber based on the 2D MoS_2 nanostructures (metamaterials) can be designed. By virtue of the surface plasmon resonance occurring at these two regions, some new types of biosensors, gas sensors, and chemical sensors are expected to be developed.

Although there have been some reports about the features of CSM and SCM in calculating the complex optical conductivities of 2D materials,[25,46,47] the applicability of these two models for 2D materials with different layers has not been investigated adequately from the perspective of experiment. In light of the experimental results, a brief discussion about the feasibility of these two models will be given. First, the differences between the complex optical conductivities obtained from these two models are calculated and plotted in Figure 3c,d.

According to previous publications,[27,28] the SCM is considered to be more suitable for a monolayer material. The feasibility of CSM in calculating the complex optical conductivity of a truly 2D material is questioned because of the lack of a rigorous definition for the complex refractive indices in a truly 2D material, and the propagation effect of light in truly 2D materials is extremely weak.[24,27,28,30] However, our experimental results suggest that the complex optical conductivities of the monolayer MoS_2 derived by these two models appear almost identical ($|\delta\sigma_r| \leq 1$ and $|\delta\sigma_r| \leq 4$) except for some slight inconsistency in the imaginary part σ_i over the high-energy region. This indicates that the CSM is also capable of assessing the complex optical conductivity of the monolayer MoS_2 with high reliability over the concerned spectral range. For the multilayer MoS_2, using the CSM to calculate the

DOI: 10.1021/acs.jpclett.9b02111
J. Phys. Chem. Lett. 2019, 10, 6246−6252

complex optical conductivity should be more advisable because the propagation effect in the multilayer MoS_2 gets stronger gradually. As shown in Figure 3c,d, the differences between the optical conductivities calculated by CSM and SCM get larger with the increasing layer number of 2D MoS_2. Specifically, with the increase of the layer number of MoS_2, the criterion $2\pi n(\omega) d/\lambda \ll 1$ that the SCM depends on is no longer satisfied,[18] and the propagation effect of the light cannot be ignored any more, thereby making SCM less and less suitable for extracting the complex optical conductivity of the multilayer 2D MoS_2, especially in the high-energy (short-wavelength) region. Thus, the differences between the optical conductivities calculated by CSM and SCM are larger in the high-energy region. The complex optical conductivities obtained by the SCM appear obviously smaller than those obtained by the CSM. These phenomena can be explained by noting that the SCM neglects the contribution of light absorption and propagation within the multilayer MoS_2 films.

Next, we will further investigate the scaling effect in the complex optical conductivity of 2D MoS_2, whose physical origin is the prominent layer-sensitive quantum confinement effect in 2D MoS_2. It can be obviously observed from Figure 3a,b that over the entire spectral range, the real parts of the complex optical conductivities σ_r for 2D MoS_2 films become larger as the thickness d increases, while the imaginary parts σ_i also present a segmented layer dependency. To some extent, σ_r represents the energy loss component caused by the light-induced conduction current, and σ_i can characterize the energy storage capacity of 2D MoS_2, which may be associated with the properties of the light-induced displacement current. The absolute values for both the real and the imaginary parts of the complex optical conductivity exhibit layer-dependent increase, indicating that the light-induced current gradually increases with the increasing layer number of 2D MoS_2. This is because the thickened MoS_2 films can provide sufficient carriers for the optoelectronic conversion process.

To further reveal the scaling effect on the optical conductivity of 2D MoS_2, we will investigate and discuss the layer-dependent shifts in the center energies of the feature peaks shown in the optical conductivity spectra. These peaks have been marked out in Figure 3a,b, and their underlying physical origins have been discussed above. For convenience, the center energies of the peaks in the real and imaginary parts of the complex optical conductivity are abbreviated as E_0^{Re} and E_0^{Im}, respectively. Specific center energies for these feature peaks, including extreme peaks and shoulder peaks, are determined by calculating the first-order and second-order differential spectra of the complex optical conductivity spectra. Specifically, the positions of extreme peaks correspond to the zero-cross points in the first-order differential curves of the complex optical conductivity spectra, whereas the center energies of those shoulder peaks are equal to the local minimums in the second-order differential curves of the optical conductivity spectra. It is worth noting that peak D in the complex optical conductivity spectra calculated by SCM cannot be exactly determined because the second-order differential spectra of the complex optical conductivities exhibit extremely drastic fluctuations. The detailed analysis method can be found in the Supporting Information. Layer-dependent center energies of these peaks are presented in Figure 4a−d. It can be seen that center energies of peaks A and B are nearly independent with the layer number L. The underlying physical origin of the layer-independent center energies of peaks A and B is that the shrinkage of the bands at the K point of the BZ and decrease of the excitonic binding energy almost cancel each other.[48,49] There is a stable splitting value of about 0.17 eV in E_0^{Re} (0.13 eV in E_0^{Im}) between the center energies of peaks A and B. The major inducement of this splitting phenomenon comes from the intralayer spin−orbit coupling (SOC) effect.[50] For peaks C and D, their center energies exhibit slight redshifts as L increases. For the high-energy peak E, the center energy exhibits an obvious layer-dependent blueshift for the imaginary part but exhibits a redshift for the real part.

We introduce the competitive mechanisms between two factors to account for these distinctive layer-dependent shifts in the optical conductivity of 2D MoS_2. One factor is the decreasing exciton binding energy as L increases, and the other is the shrinkage of the bands when the MoS_2 film undergoes a transition from the monolayer to the multilayer. The driving mechanisms of these two factors on the center energies of these peaks have been schematically illustrated in Figure 4e−g. Here, $E_{Exciton}$, E_b, and E_g are the exciton transition energy, the exciton binding energy, and the energy gap between the CB and the VB, respectively. As a reference, we assume the case in Figure 4e as the default condition for the local electronic band structure of the monolayer MoS_2. The exciton ground states (dashed black lines) are taken into account in Figure 4e−g. With the increase of L, E_b and E_g will decrease with different magnitudes. It is worth noting that the decreasing E_b will enlarge $E_{Exciton}$, while the decreasing E_g will reduce $E_{Exciton}$. Thus, the final value of $E_{Exciton}$ for a 2D MoS_2 film with a specified L hinges on the relative changes of E_b and E_g. Because the feature peaks in the optical conductivity spectra of 2D MoS_2 exhibit intense excitonic behavior, the center energies of these peaks are approximately equal to the value of $E_{Exciton}$. In this view, we can make the following inferences: When the change of E_b is larger than that of E_g as shown in Figure 4f, $E_{Exciton}$ increases, resulting in a blueshift in the center energy of the feature peak. In contrast, when the change of E_b is smaller than that of E_g as shown in Figure 4g, $E_{Exciton}$ is reduced, leading to a redshift in the center energy of the feature peak. When the changes in E_b and E_g are equal to each other, the center energy remains unchanged just like the cases of peaks A and B. On the basis of the above analysis and discussion, we can deduce that the redshifts in center energies of peaks C and D are associated with the striking contractive energy gaps between CBs and VBs. Given that the exciton effect in the high-energy peak E is more sensitive to the layer number, we conjecture the blue-shifted E_0^{Re} may be due to the fast decaying exciton binding energies. However, the abnormal redshift in E_0^{Im} of peak E cannot be explained by the above competition mechanisms, whose physical origin needs to be further investigated.

In summary, by combining SE with the CSM and the SCM, we extract the complex optical conductivities of 2D MoS_2 with different layers over an ultrabroad spectral range (0.73−6.42 eV) and further investigate their layer-dependent evolution mainly induced by the scaling effect. Five feature peaks (A−E) are observed in the complex conductivity spectra, and their center energies exhibit different intriguing layer dependencies. As the layer number increases, the center energies of peaks A and B remain unchanged, and the center energies of peaks C and D exhibit redshifts. For the high-energy peak E, the center energy of the real part exhibits a blueshift with the layer number increasing, while the center energy of the imaginary

DOI: 10.1021/acs.jpclett.9b02111
J. Phys. Chem. Lett. 2019, 10, 6246−6252

part shows an abnormal redshift. We attribute most of these novel layer-dependent evolutions to the alternative domination of the decreasing exciton binding energy and the band renormalization as the 2D MoS_2 film undergoes a transition from the monolayer to multilayer. Moreover, the applicability of the CSM and the SCM in evaluating the complex optical conductivity of 2D MoS_2 with different layers is discussed from the point of view of experiments for the first time. We find that the complex optical conductivity of the monolayer MoS_2 obtained from the CSM is nearly equal to that of the SCM, especially in low-energy regions. For the multilayer (especially $L \geq 5$), because the infinite thin sheet hypothesis in the SCM is no longer consistent with the actual film thickness, the SCM is less reliable than the CSM in evaluating complex optical conductivity of 2D MoS_2.

EXPERIMENTAL METHODS

Sample Preparation and Characterization. Wafer-scale, high-quality, layer-controllable MoS_2 films are prepared by an approach called the two-step method.[12,33] The ultrathin and uniform MoO_3 films are deposited on a sapphire substrate by an electron gun, and then the 2D MoS_2 is obtained by a subsequent sulfuration process with gaseous H_2S. The layer number of the 2D MoS_2 can be controlled by adjusting the thickness of precursor MoO_3. The Raman spectra of the MoS_2 specimens were measured by using an argon ion laser Raman spectrometer (LabRAM HR800, Horiba JobinYvon); the wavelength of the detection laser is 532 nm. A TEM system (JEOL ARM200F) and an atomic force microscope (Bruker Dimension ICON) were used to check the thicknesses and surface roughness of the MoS_2 films. A commercial SE (ME-L Mueller matrix ellipsometer, Wuhan Eoptics Technology Co., China) was used to investigate the optical conductivities of MoS_2 specimens, whose applicable energy region covers 0.73–6.42 eV.[37,38] The probing spot diameter of the ellipsometer could be as small as 200 μm by using a pair of focusing probes. Multi-incidence measurement mode was performed to reduce correlations among the fitting parameters, and the incident angles were chosen as 60°, 65°, and 70°.

ASSOCIATED CONTENT

Supporting Information

The Supporting Information is available free of charge on the ACS Publications website at DOI: 10.1021/acs.jpclett.9b02111.

Basic principles of ellipsometry and the experiment setup; ellipsometric analysis results of the 2D MoS_2 with different layers; complex refractive indices of the 2D MoS_2 with different layers; determination of the feature peaks in the optical conductivity; photoluminescence of 2D MoS_2 (PDF)

AUTHOR INFORMATION

Corresponding Authors

*E-mail: hongganggu@hust.edu.cn.
*E-mail: shyliu@hust.edu.cn.

ORCID

Hao Jiang: 0000-0003-0561-5058
Shiyuan Liu: 0000-0002-0756-1439

Notes

The authors declare no competing financial interest.

ACKNOWLEDGMENTS

This work was funded by the National Natural Science Foundation of China (Grant Nos. 51727809, 51805193, 51525502, and 51775217), the China Postdoctoral Science Foundation (Grant Nos. 2016M602288 and 2017T100546), and the National Science and Technology Major Project of China (Grant No. 2017ZX02101006-004).

REFERENCES

(1) Manzeli, S.; Ovchinnikov, D.; Pasquier, D.; Yazyev, O. V.; Kis, A. 2D Transition Metal Dichalcogenides. *Nat. Rev. Mater.* **2017**, *2*, 17033.
(2) Liu, B.; Zhou, K. Recent Progress on Graphene-Analogous 2D Nanomaterials: Properties, Modeling and Applications. *Prog. Mater. Sci.* **2019**, *100*, 99–169.
(3) Jariwala, D.; Sangwan, V. K.; Lauhon, L. J.; Marks, T. J.; Hersam, M. C. Emerging Device Applications for Semiconducting Two-Dimensional Transition Metal Dichalcogenides. *ACS Nano* **2014**, *8*, 1102–1120.
(4) Wang, Q.; Zadeh, K. K.; Kis, A.; Coleman, J. N.; Strano, M. S. Electronics and Optoelectronics of Two-Dimensional Transition Metal Dichalcogenides. *Nat. Nanotechnol.* **2012**, *7*, 699–712.
(5) Woodward, R. I.; Kelleher, E. J. R.; Howe, R. C. T.; Hu, G.; Torrisi, F.; Hasan, T.; Popov, S. V.; Taylor, J. R. Tunable Q-switched Fiber Laser Based on Saturable Edge-State Absorption in Few-Layer Molybdenum Disulfide (MoS_2). *Opt. Express* **2014**, *22*, 31113–21122.
(6) Jariwala, D.; Sangwan, V. K.; Late, D. J.; Johns, J. E.; Dravid, V. P.; Marks, T. J.; Lauhon, L. J.; Hersam, M. C. Band-Like Transport in High Mobility Unencapsulated Single-Layer MoS_2 Transistors. *Appl. Phys. Lett.* **2013**, *102*, 173107.
(7) Novoselov, K. S.; Jiang, D.; Schedin, F.; Booth, T. J.; Khotkevich, V. V.; Morozov, S. V.; Geim, A. K. Two-Dimensional Atomic Crystals. *Proc. Natl. Acad. Sci. U. S. A.* **2005**, *102*, 10451–10453.
(8) Tan, C.; Cao, X.; Wu, X.-J.; He, Q.; Yang, J.; Zhang, X.; Chen, J.; Zhao, W.; Han, S.; Nam, G.-H.; et al. Recent Advances in Ultrathin Two-Dimensional Nanomaterials. *Chem. Rev.* **2017**, *117*, 6225–6331.
(9) Boandoh, S.; Choi, S. H.; Park, J.-H.; Park, S. Y.; Bang, S.; Jeong, M. S.; Lee, J. S.; Kim, H. J.; Yang, W.; Choi, J.-Y.; et al. A Novel and Facile Route to Synthesize Atomic-Layered MoS_2 Film for Large-Area Electronics. *Small* **2017**, *13*, 1701306.
(10) Vu, Q. A.; Kim, H.; Nguyen, V. L.; Won, U. Y.; Adhikari, S.; Kim, K.; Lee, Y. H.; Yu, W. J. A High-On/Off-Ratio Floating-Gate Memristor Array on a Flexible Substrate via CVD-Grown Large-Area 2D Layer Stacking. *Adv. Mater.* **2017**, *29*, 1703363.
(11) Mak, K. F.; Shan, J. Photonics and Optoelectronics of 2D Semiconductor Transition Metal Dichalcogenides. *Nat. Photonics* **2016**, *10*, 216–226.
(12) Song, B.; Gu, H.; Fang, M.; Chen, X.; Jiang, H.; Wang, R.; Zhai, T.; Ho, Y.-T.; Liu, S. Layer-Dependent Dielectric Function of Wafer-Scale 2D MoS_2. *Adv. Opt. Mater.* **2019**, *7*, 1801250.
(13) Mak, K. F.; Lee, C.; Hone, J.; Shan, J.; Heinz, T. F. Atomically Thin MoS_2: A New Direct-Gap Semiconductor. *Phys. Rev. Lett.* **2010**, *105*, 136805.
(14) Funke, S.; Miller, B.; Parzinger, E.; Thiesen, P.; Holleitner, A. W.; Wurstbauer, U. Imaging Spectroscopic Ellipsometry of MoS_2. *J. Phys.: Condens. Matter* **2016**, *28*, 385301.
(15) Yu, Y.; Yu, Y.; Cai, Y.; Li, W.; Gurarslan, A.; Peelaers, H.; Aspnes, D. E.; Van de Walle, C. G.; Nguyen, N. V.; Zhang, Y.-W.; et al. Exciton-Dominated Dielectric Function of Atomically Thin MoS_2 Films. *Sci. Rep.* **2015**, *5*, 16996.
(16) Li, W.; Birdwell, A. G.; Amani, M.; Burke, R. A.; Ling, X.; Lee, Y. H.; Liang, X. L.; Peng, L. M.; Richter, C. A.; Kong, J.; et al. Broadband Optical Properties of Large-Area Monolayer CVD Molybdenum Disulfide. *Phys. Rev. B: Condens. Matter Mater. Phys.* **2014**, *90*, 195434.

DOI: 10.1021/acs.jpclett.9b02111
J. Phys. Chem. Lett. 2019, 10, 6246–6252

(17) Shen, C. C.; Hsu, Y. T.; Li, L. J.; Liu, H. L. Charge Dynamics and Electronic Structures of Monolayer MoS_2 Films Grown by Chemical Vapor Deposition. *Appl. Phys. Express* **2013**, *6*, 125801.
(18) Li, Y.; Chernikov, A.; Zhang, X.; Rigosi, A.; Hill, H. M.; van der Zande, A. M.; Chenet, D. A.; Shih, E.; Hone, J.; Heinz, T. F. Measurement of the Optical Dielectric Function of Monolayer Transition-Metal Dichalcogenides: MoS_2, $MoSe_2$, WS_2, and WSe_2. *Phys. Rev. B: Condens. Matter Mater. Phys.* **2014**, *90*, 205422.
(19) Zhang, H.; Ma, Y.; Wan, Y.; Rong, X.; Xie, Z.; Wang, W.; Dai, L. Measuring the Refractive Index of Highly Crystalline Monolayer MoS_2 with High Confidence. *Sci. Rep.* **2015**, *5*, 8440.
(20) Mukherjee, B.; Tseng, F.; Gunlycke, D.; Amara, K. K.; Eda, G.; Simsek, E. Complex Electrical Permittivity of the Monolayer Molybdenum Disulfide (MoS_2) in Near UV and Visible. *Opt. Mater. Express* **2015**, *5*, 447.
(21) Shen, W.-C.; Chen, R.-S.; Huang, Y.-S. Photoconductivities in MoS_2 Nanoflake Photoconductors. *Nanoscale Res. Lett.* **2016**, *11*, 124.
(22) Jariwala, D.; Davoyan, A. R.; Wong, J.; Atwater, H. A. Van Der Waals Materials for Atomically-Thin Photovoltaics: Promise and Outlook. *ACS Photonics* **2017**, *4* (12), 2962−2970.
(23) Koppens, F. H. L.; Mueller, T.; Avouris, Ph.; Ferrari, A. C.; Vitiello, M. S.; Polini, M. Photodetectors Based on Graphene, Other Two-Dimensional Materials and Hybrid Systems. *Nat. Nanotechnol.* **2014**, *9*, 780−792.
(24) Merano, M. Fresnel Coefficients of a Two-Dimensional Atomic Crystal. *Phys. Rev. A: At., Mol., Opt. Phys.* **2016**, *93*, 013832.
(25) Li, Y.; Heinz, T. F. Two-Dimensional Models for the Optical Response of Thin Films. *2D Mater.* **2018**, *5*, 025021.
(26) Jia, G. Y.; Liu, Y.; Gong, J. Y.; Lei, D. Y.; Wang, D. L.; Huang, Z. X. Excitonic Quantum Confinement Modified Optical Conductivity of Monolayer and Few-Layered MoS_2. *J. Mater. Chem. C* **2016**, *4*, 8822−8828.
(27) Chang, Y.-C.; Liu, C.-H.; Liu, C.-H.; Zhong, Z.; Norris, T. B. Extracting the Complex Optical Conductivity of Mono- and Bilayer Graphene by Ellipsometry. *Appl. Phys. Lett.* **2014**, *104*, 261909.
(28) Jayaswal, G.; Dai, Z.; Zhang, X.; Bagnarol, M.; Martucci, A.; Merano, M. Measurement of the Surface Susceptibility and the Surface Conductivity of Atomically Thin MoS_2 by Spectroscopic Ellipsometry. *Opt. Lett.* **2018**, *43*, 703−706.
(29) Liang, W. Y. Optical Anisotropy in Layer Compounds. *J. Phys. C: Solid State Phys.* **1973**, *6*, 551−565.
(30) Morozov, Y. V.; Kuno, M. Optical Constants and Dynamic Conductivities of Single Layer MoS_2, $MoSe_2$, and WSe_2. *Appl. Phys. Lett.* **2015**, *107*, 083103.
(31) Wang, H.; Zhang, C.; Rana, F. Surface Recombination Limited Lifetimes of Photoexcited Carriers in Few-Layer Transition Metal Dichalcogenide MoS_2. *Nano Lett.* **2015**, *15*, 8204−8210.
(32) Ridolfi, E.; Lewenkopf, C. H.; Pereira, V. M. Excitonic Structure of the Optical Conductivity in MoS_2 Monolayers. *Phys. Rev. B: Condens. Matter Mater. Phys.* **2018**, *97*, 205409.
(33) Matthes, L.; Pulci, O.; Bechstedt, F. Optical Properties of Two-Dimensional Honeycomb Crystals Graphene, Silicene, Germanene, and Tinene from First Principles. *New J. Phys.* **2014**, *16*, 105007.
(34) Ho, Y.-T.; Ma, C.-H.; Luong, T.-T.; Wei, L.-L.; Yen, T.-C.; Hsu, W.-T.; Chang, W.-H.; Chu, Y.-C.; Tu, Y.-Y.; Pande, K. P.; et al. Layered MoS_2 Grown on *c*-Sapphire by Pulsed Laser Deposition. *Phys. Status Solidi RRL* **2015**, *9*, 187−191.
(35) Liu, K. K.; Zhang, W.; Lee, Y. H.; Lin, Y. C.; Chang, M. T.; Su, C. Y.; Chang, C. S.; Li, H.; Shi, Y.; Zhang, H.; et al. Growth of Large-Area and Highly Crystalline MoS_2 Thin Layers on Insulating Substrates. *Nano Lett.* **2012**, *12*, 1538−1544.
(36) Lee, C.; Yan, H.; Brus, L. E.; Heinz, T. F.; Hone, J.; Ryu, S. Anomalous Lattice Vibrations of Single and Few-Layer MoS_2. *ACS Nano* **2010**, *4*, 2695−2700.
(37) Liu, S.; Chen, X.; Zhang, C. Development of a Broadband Mueller Matrix Ellipsometer as a Powerful Tool for Nanostructure Metrology. *Thin Solid Films* **2015**, *584*, 176−185.
(38) Gu, H.; Chen, X.; Jiang, H.; Zhang, C.; Liu, S. Optimal Broadband Mueller Matrix Ellipsometer Using Multi-Waveplates with Flexibly Oriented Axes. *J. Opt.* **2016**, *18*, 025702.
(39) Song, B.; Gu, H.; Zhu, S.; Jiang, H.; Chen, X.; Zhang, C.; Liu, S. Broadband Optical Properties of Graphene and HOPG Investigated by Spectroscopic Mueller Matrix Ellipsometry. *Appl. Surf. Sci.* **2018**, *439*, 1079−1087.
(40) Nelson, F. J.; Kamineni, V. K.; Zhang, T.; Comfort, E. S.; Lee, J. U.; Diebold, A. C. Optical Properties of Large-Area Polycrystalline Chemical Vapor Deposited Graphene by Spectroscopic Ellipsometry. *Appl. Phys. Lett.* **2010**, *97*, 253110.
(41) Carvalho, A.; Ribeiro, R. M.; Neto, A. H. C. Band Nesting and the Optical Response of Two-Dimensional Semiconducting Transition Metal Dichalcogenides. *Phys. Rev. B: Condens. Matter Mater. Phys.* **2013**, *88*, 115205.
(42) Maurya, J. B.; Prajapati, Y. K.; Singh, V.; Saini, J. P.; Tripathi, R. Improved Performance of the Surface Plasmon Resonance Biosensor Based on Graphene or MoS_2 Using Silicon. *Opt. Commun.* **2016**, *359*, 426−434.
(43) Mishra, A. K.; Mishra, S. K.; Verma, R. K. Graphene and Beyond Graphene MoS_2: A New Window in Surface-Plasmon-Resonance-Based Fiber Optic Sensing. *J. Phys. Chem. C* **2016**, *120*, 2893−2900.
(44) Beal, A. R.; Hughes, H. P. Kramers-Kronig Analysis of the Reflectivity Spectra of 2H-MoS_2, 2H-$MoSe_2$, and 2H-$MoTe_2$. *J. Phys. C: Solid State Phys.* **1979**, *12*, 881−890.
(45) Beal, A. R.; Liang, W. Y.; Hughes, H. P. Kramers-Kronig Analysis of the Reflectivity Spectra of 3R-WS_2 and 2H-WSe_2. *J. Phys. C: Solid State Phys.* **1976**, *9*, 2449−2457.
(46) Majérus, B.; Dremetsika, E.; Lobet, M.; Henrard, L.; Kockaert, P. Electrodynamics of Two-Dimensional Materials: Role of Anisotropy. *Phys. Rev. B: Condens. Matter Mater. Phys.* **2018**, *98*, 125419.
(47) Matthes, L.; Pulci, O.; Bechstedt, F. Influence of Out-Of-Plane Response on Optical Properties of Two-Dimensional Materials: First Principles Approach. *Phys. Rev. B: Condens. Matter Mater. Phys.* **2016**, *94*, 205408.
(48) Molina-Śanchez, A.; Sangalli, D.; Hummer, K.; Marini, A.; Wirtz, L. Effect of Spin-Orbit Interaction on the Optical Spectra of Single-Layer, Double-Layer, and Bulk MoS_2. *Phys. Rev. B: Condens. Matter Mater. Phys.* **2013**, *88*, 045412.
(49) Koperski, M.; Molas, M. R.; Arora, A.; Nogajewski, K.; Slobodeniuk, A. O.; Faugeras, C.; Potemski, M. Optical Properties of Atomically Thin Transition Metal Dichalcogenides: Observations and Puzzles. *Nanophotonics* **2017**, *6*, 1289−1308.
(50) Fan, X.; Singh, D. J.; Zheng, W. Valence Band Splitting on Multilayer MoS_2: Mixing of Spin-Orbit Coupling and Interlayer Coupling. *J. Phys. Chem. Lett.* **2016**, *7*, 2175−2181.

DOI: 10.1021/acs.jpclett.9b02111
J. Phys. Chem. Lett. 2019, 10, 6246−6252

Supporting Information

Complex Optical Conductivity of 2D MoS_2: A Striking Layer-Dependency

Baokun Song,[†] Honggang Gu,[†,] Mingsheng Fang,[†] Yen-Teng Ho,[‡] Xiuguo Chen,[†] Hao Jiang,[†] Shiyuan Liu[†,*]*

[†]State Key Laboratory of Digital Manufacturing Equipment and Technology, Huazhong University of Science and Technology, Wuhan 430074, Hubei, China

[‡]Department of Materials Science and Engineering, National Chiao Tung University, Hsinchu 30010, Taiwan, China

Corresponding Authors

[*]E-mail: hongganggu@hust.edu.cn

[*]E-mail: shyliu@hust.edu.cn

Basic principles of ellipsometry and the experimental set-up

Ellipsometry is a widely used optical technique that can simultaneously gain the optical and geometrical parameters of nanofilms and nanomaterials in a nondestructive manner by detecting the polarization state changes of the light after interacting with the samples.[1-3] As shown in Figure S1a, the polarization state changes are usually described by two ellipsometric angles $\{\Psi(\omega), \Delta(\omega)\}$ (ω: the angular frequency of light), which can be expressed as

$$\tan\Psi \cdot \exp(\mathrm{i}\Delta) = r_\mathrm{p} / r_\mathrm{s}, \tag{S1}$$

where, $\tan\Psi$ and Δ represent amplitude ratio and phase difference between the *p*- and *s*-components of the polarized light respectively, and r_p and r_s refer to the amplitude reflection coefficients for *p*-polarization and *s*-polarization, which can be written as

$$r_\mathrm{p} / r_\mathrm{s} = (\mathbf{E}_\mathrm{rp} / \mathbf{E}_\mathrm{ip}) / (\mathbf{E}_\mathrm{rs} / \mathbf{E}_\mathrm{is}). \tag{S2}$$

Here, $\mathbf{E}_\mathrm{ip}$ and $\mathbf{E}_\mathrm{is}$ represent the electric field vectors of incident *p*- and *s*-polarizations, and $\mathbf{E}_\mathrm{rp}$ and $\mathbf{E}_\mathrm{rs}$ represent the electric field vectors of reflected *p*- and *s*-polarizations (Figure S1a).

Figure S1b gives a photograph of the spectroscopic ellipsometer (ME-L Mueller matrix ellipsometer from Wuhan E-optics Technology Co., China) used in our work.[2,3] It contains a light source, a polarization state generator (PSG), a sample stage, a polarization state analyzer (PSA), and a detector. The PSG modulates the polarization state of the light emitted from the light source, while the PSA demodulates the polarization state of the light after reacting with the samples. The ellipsometric spectra $\{\Psi(\omega), \Delta(\omega)\}$ can be obtained by analyzing the light intensity signals recorded by the detector. The ellipsometer covers an energy range of

0.73–6.42 eV. In the experiments, multi-incidence measurement mode is chosen to reduce correlations among the fitting parameters with the incident angles set as 60°, 65°, and 70°. The diameter of the probing spot can be focused to 200 μm by using a pair of focusing probes. It is helpful for the measurement of some submillimeter samples.

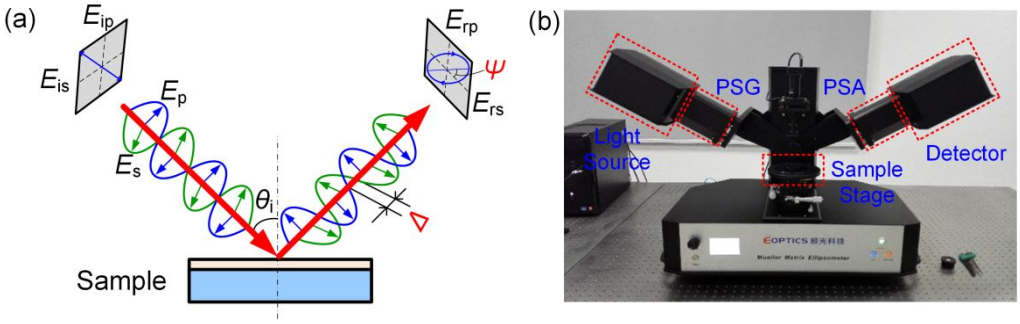

Figure S1. (a) Basic principles of ellipsometry. (b) A photograph of the experimental set-up.

Ellipsometric analysis of 2D MoS_2

Ellipsometry is a model-based technique. To analyze the measured ellipsometric spectra, two models need to be constructed, namely the optical model and the dielectric function model. The optical model describes the light propagation through the optical stack of the sample calculated by the transfer matrix method. While the dielectric function model gives the dispersive properties of the material which would be involved in the optical model. The theoretical ellipsometric spectra of the sample can be calculated with the above two models.[1] By fitting the measured ellipsometric spectra with the theoretical calculated ones, the basic optical parameters (such as the complex refractive index and the dielectric function) and geometrical parameters (such as the thickness and the surface roughness) of the sample can be obtained simultaneously.

The optical model for the 2D MoS_2 samples is a vertical stacking multilayer structure, including the ambient air, the 2D MoS_2, the Bruggeman interlayer, and the sapphire substrate (Figure S2). The Bruggeman interlayer contains 50% 2D MoS_2 and 50% sapphire substrate, which can effectively describe the transition interface between two materials.[1] The goodness of the ellipsometric fit can be further improved by introducing the Bruggeman interlayer. A generalized oscillator model combining a Cody-Lorentz oscillator and five Lorentz oscillators is used to embody the dielectric properties of the 2D MoS_2.[1,4,5] On the basic of the above two models, the theoretical ellipsometric spectra of the 2D MoS_2 can be calculated. Figure S3 illustrates the measured and best-fitting ellipsometric spectra of the 2D MoS_2 with different layers. Obviously, the theoretical ellipsometric spectra are in good agreement with the experimental ellipsometric spectra, indicating that the models established by us are reasonable.

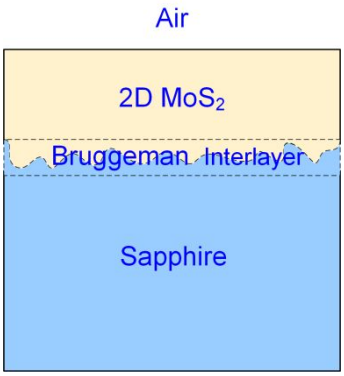

Figure S2. Optical model of the 2D MoS_2 on sapphire substrate used in the ellipsometric analysis.

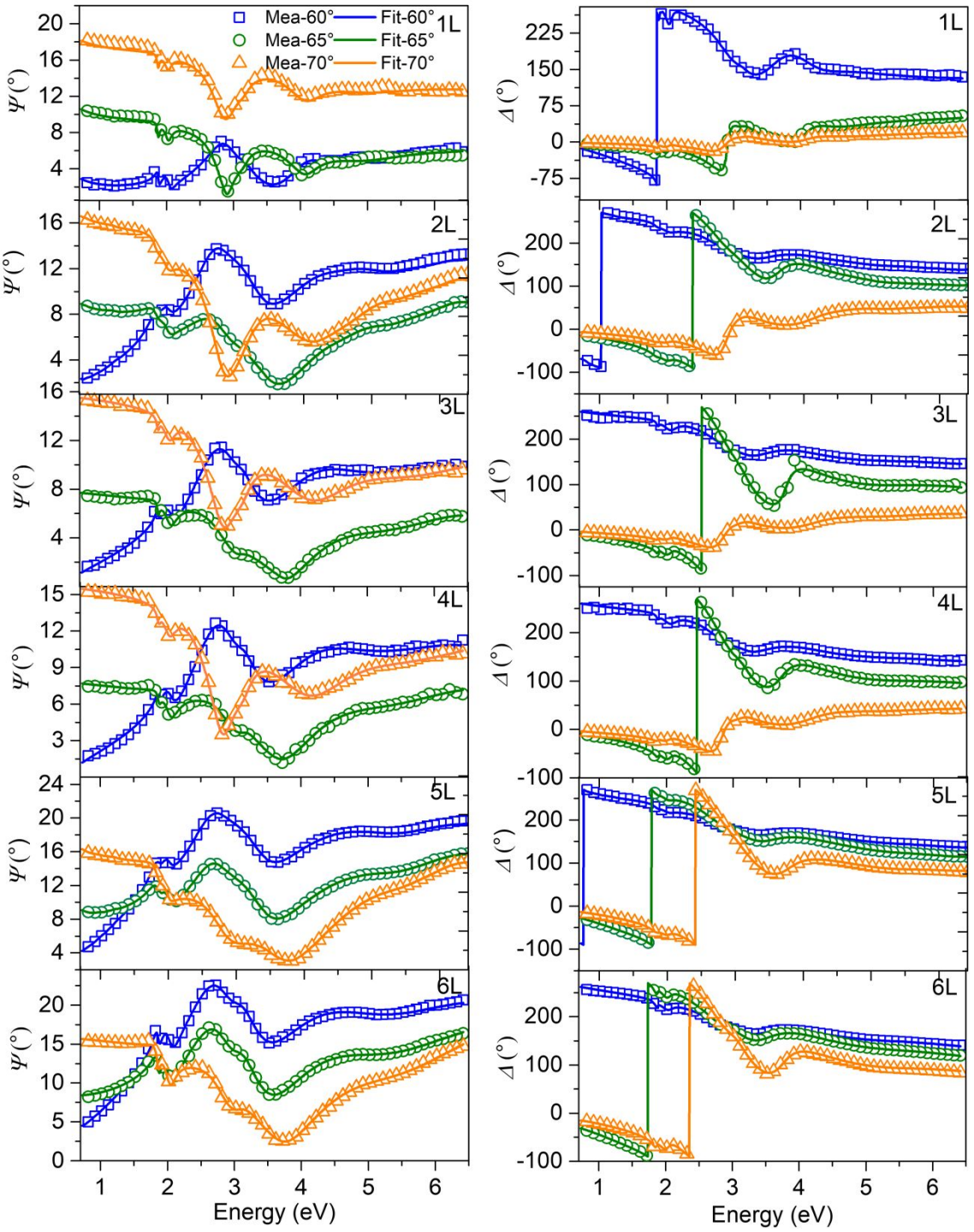

Figure S3. Measured and best fitting ellipsometric spectra $\{\Psi(\omega), \Delta(\omega)\}$ of the 1–6L MoS_2 on the sapphire substrates.

Complex refractive index of 2D MoS_2

Figures S4a,b demonstrate the complex refractive indices, including the refractive indices n and the extinction coefficients κ, of the 2D MoS_2 films with different layers extracted from the measured ellipsometric spectra. The complex optical indices of the 2D MoS_2 exhibits non-monotonic layer-dependencies due to the competition between the decreasing exciton effect and increasing joint density of state (JDOS).[6] This competition reaches a balance when the layer number of 2D MoS_2 is about 3–4, which may be the main reason for the similar complex refractive indices of 3L and 4L MoS_2. The absorption peaks appearing on the extinction coefficient spectra are associated with the optical transitions and the prominent exciton effect in 2D-MoS_2.[7] The first two peaks in the low-energy region can be assigned to the direct transitions from the first valance band (VB) and its quantized subband to the conductive band (CB) minimum at the K point of the Brillouin zone (BZ).[8] The splitting quantized subband is related to the quantum confinement in the out-of-plane direction (the direction parallel to the c-axis of the MoS_2).[9] For those peaks in the high-energy interval, broad full widths at half maximum indicate that the multiple-transition behavior may play a major role in the formations of these peaks. The thicknesses of 1–6L MoS_2 specimens measured by SE are 0.60 nm, 1.15 nm, 1.89 nm, 2.40 nm, 3.05 nm, and 3.53 nm, respectively.

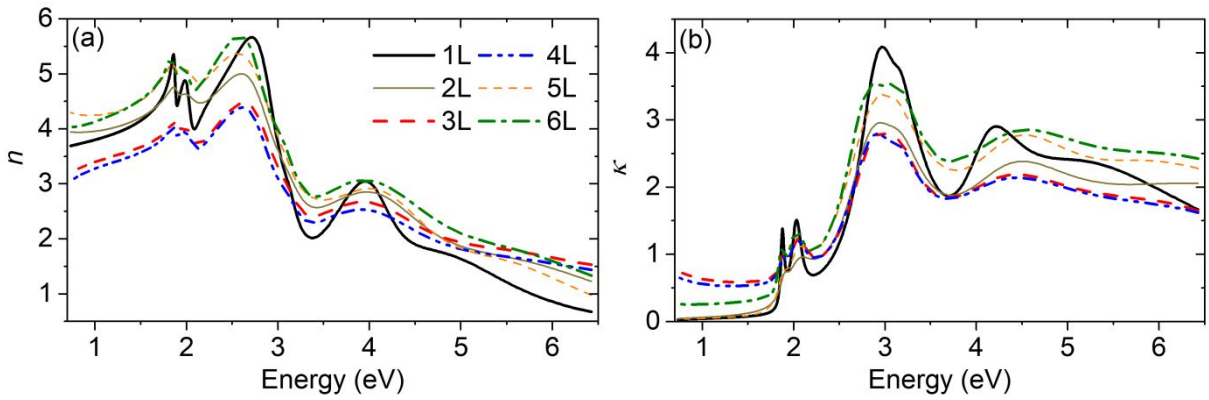

Figure S4. Complex refractive indices of 1–6L MoS_2. (a) Refractive indices. (b) Extinction coefficients.

Determination of feature peaks in the optical conductivity of 2D MoS_2

The center energies of the feature peaks in optical conductivity spectra of the 2D MoS_2 can be determined by analyzing zero-cross points in the first-order and the local minimums in the second-order differential spectra of the optical conductivity spectra. As shown in Figure S5a–f and Figure S6a–f, the black (blue) solid lines represent the first-order differential spectra of the real (imaginary) parts of the complex optical conductivity spectra for the 1–6L MoS_2. The center energies of the extreme peaks A, B, C, and E in the optical conductivity spectra (Figure 3a,b) correspond to the positive-to-negative zero-cross points with the increasing energy. As shown in Figure S5a–f and Figure S6a–f, the zero-cross points marked by red (green) dots are equal to the center energies of the extreme peaks in the real (imaginary) parts of the optical conductivity spectra. For the special shoulder peak D in Figure 3a,b, its center energies are equal to the local minimums in the second-order differential spectra of the complex optical conductivities. However, the specific positions of

peak D in the complex optical conductivity spectra calculated by SCM cannot be determined according to the above methods because the second-order differential spectra of the complex optical conductivities exhibit extremely drastic fluctuations. Specifically, the complex optical conductivity spectra obtained by the SCM are calculated from the measured ellipsometric spectra wavelength by wavelength, which inevitably contain some environmental random noise. When we calculate the second-order differential spectra of the of the complex optical conductivities, the local fluctuating noise signals are extremely amplified and prevent us from finding the local minimum in the second-order differential spectra. The fluctuation phenomena can also be observed in the first-order differential spectra of the complex optical conductivities obtained by SCM, as shown in Figure S6a–f. Fortunately, these fluctuations are not very drastic in the first-order differential spectra. According to the overall trends of these fluctuation curves, we roughly mark the positions of feature peaks A, B, C, and E. The center energies of peaks A–E in the real and imaginary parts of the optical conductivity spectra calculated by CSM and SCM are summarized in Table S1 and Table S2.

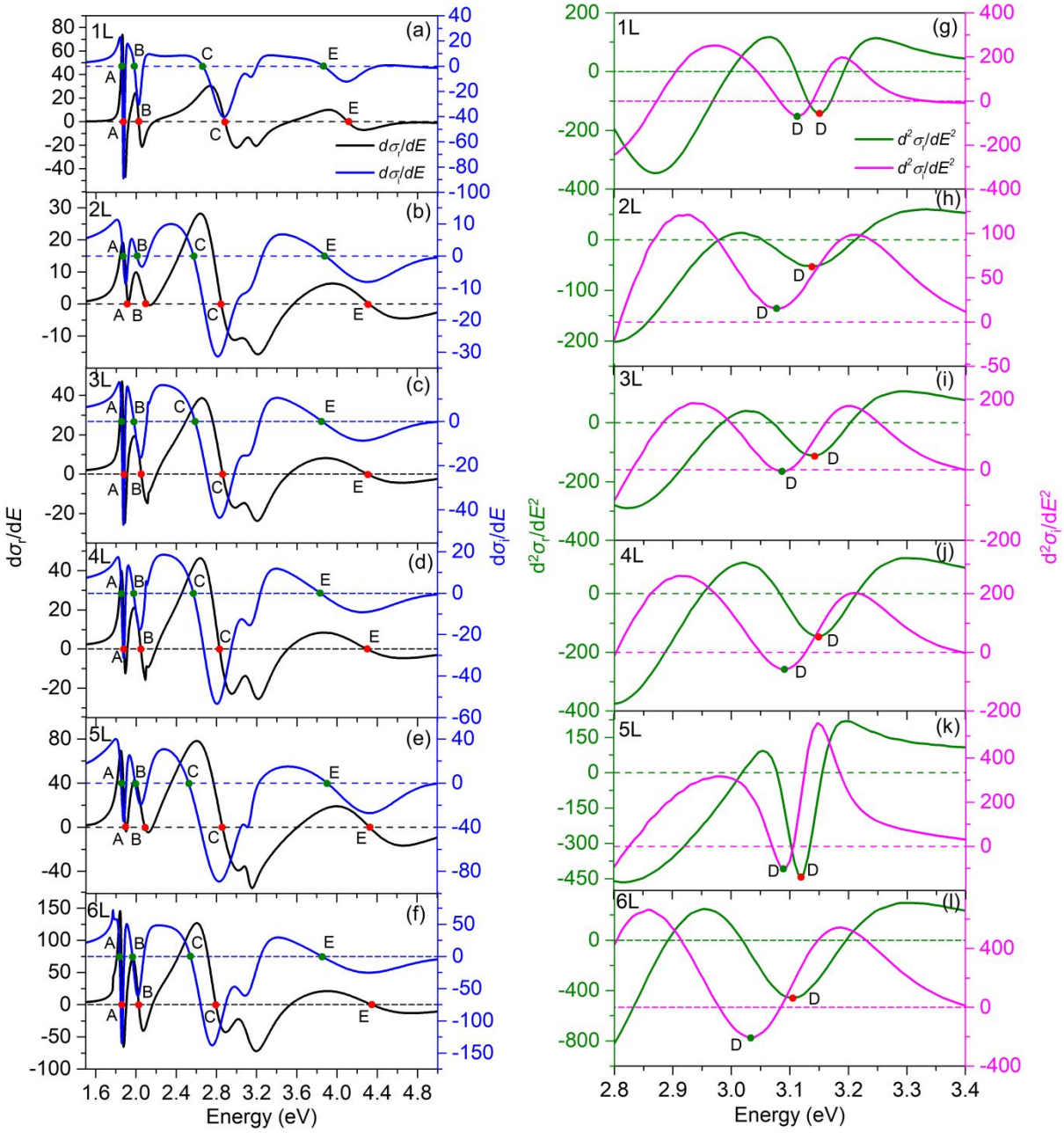

Figure S5. Differential spectra of CSM calculated complex optical conductivities of 1–6L MoS_2. (a–f) First-order differential spectra. (g–l) Second-order differential spectra.

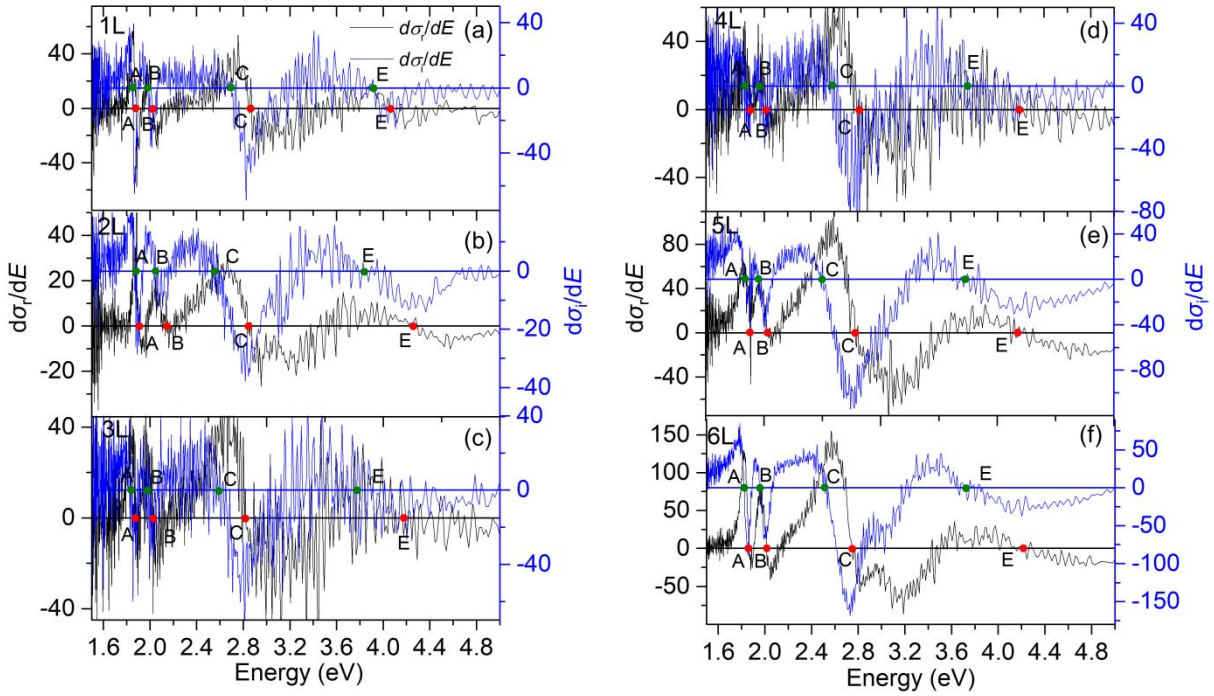

Figure S6. First-order differential spectra of SCM calculated complex optical conductivities of 1–6L MoS_2.

Photoluminescence of 2D MoS_2

To further confirm the layer-dependency that the complex optical conductivity spectra of the 2D MoS_2 exhibits, the photoluminescence (PL) spectra of 1–6L MoS_2 are measured and uniformly plotted in Figure S7a. It is obvious that there are two feature PL peaks (A and B) in Figure S7a, which correspond the first two feature peaks in the complex optical conductivity spectra of the 2D MoS_2. The center energies of the PL peaks A and B in the monolayer MoS_2 are slightly larger than those of the non-monolayer MoS_2. This can be mainly attributed to that the non-monolayer MoS_2 is indirect bandgap semiconductor whose indirect bandgap is smaller than the direct bandgap of the monolayer MoS_2. To some extent, the PL response

from the indirect bandgap causes the redshift of the peak A in the PL spectrum of the non-monolayer MoS_2. As illustrated in Figure S7b, the positions of peaks A and B in the PL spectra of the 2D MoS_2 also exhibit insignificant layer-dependencies, which are consistent with the layer-independencies that the complex optical conductivity of the 2D MoS_2 exhibits (Figure 4a–d).

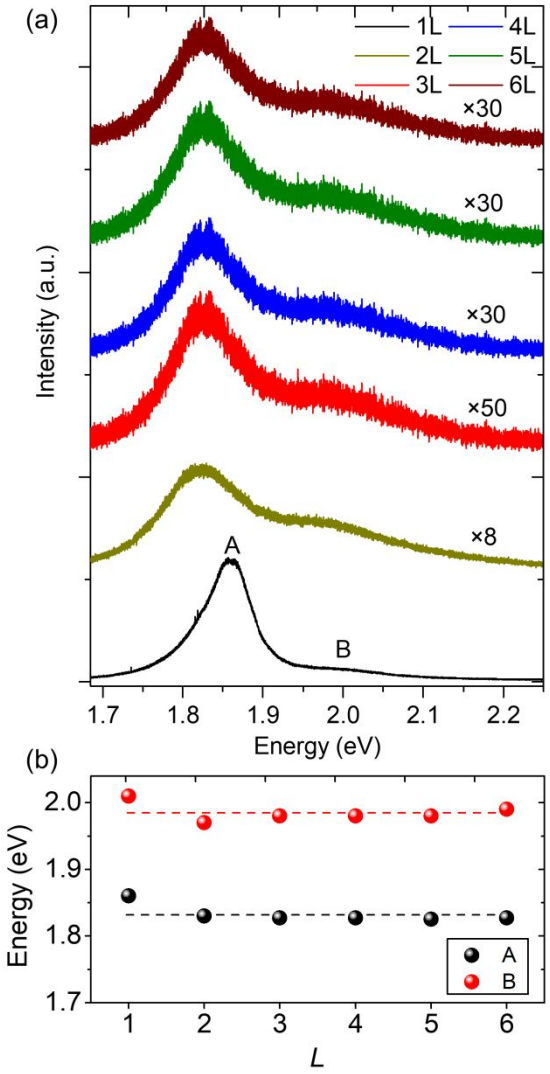

Figure S7. (a) Photoluminescence of 1–6L MoS_2, the wavelength of the detection laser is 514nm. (b) Center energies of PL peaks A and B versus the layer number of 2D MoS_2.

Table S1. Feature peaks (A–E) in the CSM calculated σ (E) of 1–6L MoS_2

L	σ_r^{CSM}					σ_i^{CSM}				
	A	B	C	D	E	A	B	C	D	E
1	1.87	2.03	2.88	3.15	4.11	1.86	1.98	2.66	3.11	3.86
2	1.90	2.09	2.85	3.14	4.32	1.87	2.00	2.58	3.08	3.86
3	1.87	2.05	2.86	3.14	4.30	1.85	1.98	2.59	3.09	3.85
4	1.88	2.05	2.83	3.14	4.30	1.85	1.98	2.57	3.09	3.84
5	1.89	2.08	2.85	3.12	4.32	1.86	2.01	2.54	3.08	3.87
6	1.86	2.03	2.80	3.11	4.34	1.84	1.97	2.54	3.03	3.83

Table S2. Feature peaks (A, B, C, E) in the SCM calculated σ (E) of 1–6L MoS_2

L	σ_r^{SCM}				σ_i^{SCM}			
	A	B	C	E	A	B	C	E
1	1.87	2.02	2.86	4.07	1.85	1.98	2.69	3.92
2	1.91	2.14	2.85	4.25	1.87	2.04	2.55	3.84
3	1.87	2.03	2.82	4.17	1.84	1.98	2.58	3.78
4	1.88	2.01	2.82	4.19	1.84	1.96	2.57	3.74
5	1.88	2.03	2.78	4.22	1.84	1.96	2.49	3.72
6	1.86	2.01	2.75	4.22	1.82	1.96	2.50	3.72

References

(1) Fujiwara, H. *Spectroscopic Ellipsometry: Principles and Applications*; *John Wiley & Sons: Chichester*, 2007; pp 81-207.

(2) Liu, S.; Chen, X.; Zhang, C. Development of a Broadband Mueller Matrix Ellipsometer as a Powerful Tool for Nanostructure Metrology. *Thin Solid Films* **2015**, *584*, 176-185.

(3) Gu, H.; Chen, X.; Jiang, H.; Zhang, C.; Liu, S. Optimal Broadband Mueller Matrix Ellipsometer Using Multi-Waveplates with Fexibly Oriented Axes. *J. Opt.* **2016**, *18*, 025702.

(4) Shen, C. C.; Hsu, Y. T.; Li, L. J.; Liu, H. L. Charge Dynamics and Electronic Structures of Monolayer MoS_2 Films Grown by Chemical Vapor Deposition. *Appl. Phys. Express* **2013**, *6*, 125801.

(5) Ferlauto, A. S.; Ferreira, G. M.; Pearce, J. M.; Wronski, C. R.; Collins, R. W.; Deng, X.; Ganguly, G. Analytical Model for The Optical Functions of Amorphous Semiconductors

from the Near-Infrared to Ultraviolet: Applications in Thin Film Photovoltaics. *J. Appl. Phys.* **2002**, *92*, 2424-2436.

(6) Song, B.; Gu, H.; Fang, M.; Chen, X.; Jiang, H.; Wang, R.; Zhai, T.; Ho, Y.-T.; Liu, S. Layer-Dependent Dielectric Function of Wafer-Scale 2D MoS_2. *Adv. Opt. Mater.* **2019**, *7*, 1801250.

(7) Li, W.; Birdwell, A. G.; Amani, M.; Burke, R. A.; Ling, X.; Lee, Y. H.; Liang, X. L.; Peng, L. M.; Richter, C. A.; Kong, J.; Gundlach, D. J.; Nguyen, N. V. Broadband Optical Properties of Large-Area Monolayer CVD Molybdenum Disulfide. *Phys. Rev. B* **2014**, *90*, 195434.

(8) Mak, K. F.; Lee, C.; Hone, J.; Shan, J.; Heinz, T. F. Atomically Thin MoS_2: A New Direct-Gap Semiconductor. *Phys. Rev. Lett.* **2010**, *105*, 136805.

(9) Zhang, G.; Chaves, A.; Huang, S.; Wang, F.; Xing, Q.; Low, T.; Yan, H. Determination of Layer-Dependent Exciton Binding Energies in Few-Layer Black Phosphorus. *Sci. Adv.* **2018**, *4*, eaap9977.